Key Points:
- Rapid shortwave cloud adjustments over central Europe in ICON-A GCM are representative of CMIP5 models over Northern Hemispheric continents
- Using present-day meteorological and CO_2 concentrations for later boundary conditions in 4xCO_2 simulations is not an issue up to 36 hr
- Shortwave rapid cloud adjustments up to 36 hr may be evaluated in large-eddy simulations

Supporting Information:
- Supporting Information S1

Correspondence to:
C. Nam,
christine.nam@uni-leipzig.de

A Prospectus for Constraining Rapid Cloud Adjustments in General Circulation Models

Christine Nam[1,2] (iD)**, Philipp Kühne[1]** (iD)**, Marc Salzmann[1]** (iD)**, and Johannes Quaas[1]** (iD)

[1]Leipzig Institute for Meteorology, Universität Leipzig, Leipzig, Germany, [2]Max Planck Institute for Meteorology, Hamburg, Germany

Abstract Rapid cloud adjustments are an important component of the atmosphere's total response to increased CO_2 concentrations. Unfortunately, scientific understanding of rapid shortwave cloud adjustments is rather poor. State-of-the-art 5th Coupled Model Intercomparison Project models showed large uncertainty in regard to rapid cloud adjustments. This study determines whether large-eddy simulations may, in principle, be used as a reference, thanks to their ability to resolve cloud dynamics and thermodynamics, to constrain rapid shortwave cloud adjustments in general circulation models. This is an open question since large-eddy models can only be run over limited domains, for a short period of time, and are influenced by boundary conditions. Using the Icosahedral Non-hydrostatic global climate model—Atmospheric component (ICON-A), we examine shortwave rapid cloud adjustments over central Europe, which is found to be representative of shortwave rapid cloud adjustments over Northern Hemispheric global continents in the 5th Coupled Model Intercomparison Project models. This work finds (i) a couple of days of simulation is sufficient to get a clear signal in the net top-of-atmosphere radiative balance to emerge after a 4xCO_2 perturbation and (ii) use of present-day meteorological and CO_2 concentrations for boundary conditions in global simulations is not an issue for short lead times, up to ~36 hr. We also found that atmospheric processes influencing shortwave rapid cloud adjustments over central Europe are largely thermodynamically driven changes in local cloud dynamics and are rather independent of the synoptic-scale and circulation effects on short timescales (<2 days). These results imply that high-resolved large-eddy simulations over a limited area can be instructive for assessing and constraining global rapid cloud adjustments.

Plain Language Summary Our work demonstrates that large-eddy simulations may, in principle, be used to constrain rapid adjustments in general circulation models despite the fact that large-eddy models can only be run on over limited area, run for a short period of time, and are influenced by boundary conditions.

1. Introduction

One of the most urgent problems in climate science is to quantify climate sensitivity, the global-mean equilibrium surface temperature response to a doubling of the atmospheric carbon dioxide (CO_2) concentration, which is hitherto highly uncertain. The uncertainty in general circulation models (GCMs) can be traced back, to a large extent, to the variable response of clouds to the CO_2 forcing, occurring at both fast (adjustments) and slow (feedbacks) timescales.

Recent studies have shown rapid adjustments to be an important component of the total cloud response to perturbations of atmospheric CO_2 concentrations (Andrews et al., 2012; Block & Mauritsen, 2013; Gregory & Webb, 2008; Kamae et al., 2015). Changes to CO_2 concentrations have an immediate effect on longwave radiative fluxes, and subsequently atmospheric profiles of temperature and relative humidity (RH) are affected, which in turn affects the evolution of clouds and shortwave radiative fluxes, and thereby the net top-of-atmosphere radiative balance (Andrews & Forster, 2008; Colman & McAvaney, 2011; Gregory & Webb, 2008; Kamae & Watanabe, 2013; Wyant et al., 2012). Changes due to the CO_2 perturbation that occur before a change in ocean surface temperatures are called rapid adjustments (Sherwood et al., 2015), and the associated changes to the net top-of-atmosphere radiative budget is called the effective radiative forcing (Boucher et al., 2013; Gregory et al., 2004; Sherwood et al., 2015). Rapid adjustments have been found to act on short timescales on the order of hours to weeks after the forcing is imposed (Bony et al., 2013; Dong et al., 2009).

Calculations of rapid cloud adjustments by climate models vary considerably (Gregory & Webb, 2008), including the GCMs participating in CMIP5 (5th Coupled Model Intercomparison Project; Taylor et al., 2012) as shown by Vial et al. (2013). Using radiative kernels, Vial et al. (2013) determined that rapid adjustments by clouds account for approximately 0.4 to 0.5 W/m^2 per doubling of CO_2, which contributes approximately 20% of the average total cloud response (Vial et al., 2013; Zelinka et al., 2013). Rapid cloud adjustments have been found to scale with CO_2 forcing rather than the global-mean temperature response; this makes the forcing term in climate sensitivity calculations uncertain and justifies including cloud adjustments in the effective radiative forcing, rather than considering them part of the cloud feedback (Sherwood et al., 2015). As such, rapid adjustments are fast, uncertain, and cardinal.

Currently, the diversity found in cloud adjustments to CO_2 perturbations in global climate models is largely due to parameterizations associated with clouds, convection, turbulence, and their interactions. This has motivated the use of large-eddy models (LEMs), which can resolve and more reliably represent these processes. Several recent studies have demonstrated that LEMs can improve our understanding of climate-relevant processes (e.g., Blossey et al., 2016; Matsueda, 2011).

LEMs, however, are driven with boundary conditions, either from idealized profiles or weather forecasts, and run over a limited area domain for short periods of time. As such, one must identify a domain which can produce the same magnitude of variability of rapid cloud adjustments found in GCMs, determine the extent which the large-scale environment influences rapid cloud adjustments through advection, and ascertain the temporal and spatial scales at which the adjustments are statistically significant.

This work will assess rapid cloud adjustments to anthropogenic CO_2 forcings in the newly developed ICON-A GCM (Icosahedral Non-hydrostatic global climate model—Atmospheric component; Giorgetta et al., 2018) of the German Weather Service (Deutscher Wetterdienst, DWD) and Max Planck Institute for Meteorology. We performed three transpose AMIP-style simulations where AMIP is the Atmospheric Model Intercomparison Project protocol, where atmospheric GCMs are driven by prescribed sea surface temperatures (SSTs) and sea ice cover but integrated only for a short period, up to 30 days in our study, after initialization in a numerical-weather prediction-type simulations. The experiments include a control AMIP experiment, a global abrupt4xCO2 experiment, and a local abrupt4xCO2 experiment in which CO_2 is only increased over central Europe (see section 2.2 for details). In order to explore the representativeness of a selected region for mean and intermodel diversity of rapid cloud adjustments, the multimodel ensemble of the CMIP5 (Taylor et al., 2012) is analyzed. Together, the CMIP5 examination and the three ICON-A experiments will allow us to investigate whether a LEM, driven with present-day meteorology at its boundaries, might be instructive for rapid cloud adjustments by addressing the following three points:

1. What is the shortest temporal scale which a statistically significant signal in shortwave rapid cloud adjustments develops in global climate model over land?
2. Can a localized perturbation in CO_2 over central Europe, defined here as 4–14.5°E, 45–56.5°N, yield an adjustment with a similar scale and variability as global adjustments? That is, is this domain approximately representative for global land areas, so that a meaningful constraint may be obtained?
3. Are shortwave rapid cloud adjustments, to CO_2 perturbations, imposed on a local scale representative of those on the global scale, or does the large-scale environment (aka boundary conditions and advection) dominate the signal?

The present work is motivated by the High-Definition Clouds and Precipitation for Climate Prediction (HD[CP]^2, http://www.hdcp2.eu) project. In the context of this project, a LEM has been developed and tested for simulations of up to a few days over the domain of central Europe (Heinze et al., 2017). This existing setup motivates the choice of the central European region defined above. The results of this study will be used to guide a study using the ICON-LEM run over central Europe that will simulate 4xCO2 perturbations and rapid cloud adjustments. Given the computational cost of a large-eddy simulation over central Europe with a horizontal resolution of $\mathcal{O}$ (100 m), which has a factor of 1,000 more grid columns over the limited domain than a typical GCM does globally, there will only be one realization of a couple of days. Therefore, it is crucial to see which part of the ICON-A GCM distribution of rapid cloud adjustments, determined from a 92-member ensemble, the ICON-LEM will capture—if any at all. Through the combination of these two studies, we hope to learn how rapid cloud adjustments manifest in a LEM, which will ultimately help constrain rapid cloud adjustments in GCMs.

This paper is structured in the following manner: Section 2 introduces the CMIP5's (Taylor et al., 2012) models used in this study, as well as the ICON-A GCM model and experimental setup. In sections 3 and 4 we demonstrate the representativeness of rapid shortwave cloud adjustments over central Europe of global adjustments, both in terms of magnitude and variability, in CMIP5 models and the new ICON-A GCM. Lastly, the discussions and conclusions are presented in sections 5 and 6, respectively.

2. Models and Experiments

Bony et al., 2013 demonstrated that short simulations with GCMs, on the order of days, were sufficient to investigate rapid cloud adjustments and their contribution to climate change. Rapid cloud adjustments are commonly quantified in two manners, as Sherwood et al. (2015) points out. There is the *regression method*, which regresses the net top-of-atmosphere flux perturbations onto temperature changes in a transient warming simulation and diagnoses the rapid adjustments at the intercept of zero global-mean temperature change, that is, at $\Delta T = 0$ (Gregory et al., 2004). There is also the *fixed SST method*, which diagnoses the effective radiative forcing from a simulation where SSTs and sea ice are prescribed (Cess & Potter, 1988; Forster et al., 2016; Hansen et al., 2005). In practice, the difference between these two definitions is how land surface temperature changes on short timescales are accounted for, but they produce similar results on average (Forster et al., 2016). In both approaches, rapid cloud adjustments are considered part of the effective radiative forcing, but the latter definition is more practical when investigating the regional pattern of rapid cloud adjustments. In particular, it avoids the ambiguity related to extrapolating radiative effects of regional cloud changes back to a zero surface temperature change intercept for the global-mean surface temperature.

In this work, we use the fixed SST method combined with a linearized radiative kernel technique to determine the strength and structure of shortwave cloud radiative adjustments in CMIP5 models over central Europe. In this method, cloud responses to surface temperature changes over land are considered part of the rapid cloud adjustments. The linearized radiative kernel technique (Shell et al., 2008) takes cloud masking effects, the apparent change in cloud feedbacks due to alteration of other climate constituents as water vapor or surface albedo, into consideration (Shell et al., 2008). This study will demonstrate that there is considerable intermodel spread in shortwave rapid cloud adjustments simulated both over central Europe and over Northern Hemisphere (NH) land areas and that the magnitudes of cloud adjustments over central Europe and of cloud adjustments over global land areas are correlated, that is, that models that show a large shortwave rapid cloud adjustment over central Europe tend to also show a large shortwave rapid cloud adjustment over global land areas.

Following the CMIP5 multimodel analysis, we use the second method to demonstrate that rapid cloud adjustments to CO_2 forcings over a limited area, specifically central Europe, are similarly representative of global adjustments within the newly developed ICON-A GCM up to ~36 hr.

Each of these studies is described further in the following two subsections.

2.1. CMIP5 Models

For the CMIP5 model comparison, output from 13 atmosphere models, representing atmospheric components of CMIP5 models, listed in Table 1, is analyzed. The differences between the monthly mean values from the sstClim4xCO2 experiment, in which atmospheric carbon dioxide concentrations of preindustrial levels are instantaneously quadrupled while SSTs are kept at preindustrial values (Taylor et al., 2012), and the sstClim experiment, in which both the CO_2 concentration and the SSTs are prescribed at preindustrial levels (Taylor et al., 2012), are calculated. Following which, a radiative kernel method is applied using the radiative kernels of Shell et al. (2008) to all 13 models, and the shortwave radiative effects of rapid cloud adjustments calculated from each model are combined to create a multimodel mean and multimodel standard deviation. For models in which the sstClim and sstClim4xCO2 experiments were run for much longer than 30 years, only the first 30 years was included in the analysis.

2.2. ICON Global Climate Model

Three transpose AMIP-style experiments have been performed with the ICON-A GCM with prescribed SSTs and sea ice coverage from observations at a resolution of R2B4 (approximately 139 km). ICON-A also has a terrain following hybrid sigma height grid following Leuenberger et al. (2010), with 47 full vertical levels, with layer thicknesses ranging from 40 m in the lowermost layers to ~300 m at 1 km, and ~1 km at 10 km (Giorgetta et al., 2018).

Table 1
List of CMIP5 Models Included in Analysis

Modeling center	Model version	Reference
BCC, China	bcc-csm1-1	Wu et al. (2010)
BNU, China	BNU-ESM	Ji et al. (2014)
CCCma, Canada	CanESM2	Arora et al. (2011)
CSIRO, Australia	ACCESS1-3	Bi et al. (2013)
CSIRO, Australia	CSIRO-Mk3.6.0	Rotstayn et al. (2012)
INM, Russia	inmcm4	Volodin et al. (2010)
IPSL, France	IPSL-CM5A-LR	Dufresne et al. (2013)
MIROC, Japan	MIROC5	Watanabe et al. (2010)
MOHC, UK	HadGEM2-A	Martin et al. (2011)
MPI-M, Germany	MPI-ESM-LR	Giorgetta et al. (2013)
MRI, Japan	MRI-CGCM3	Yukimoto et al. (2012)
NCAR, United States	CCSM4	Gent et al. (2011)
NCC, Norway	NorESM1-M	Bentsen et al. (2013)

Note. CMIP5 = 5th Coupled Model Intercomparison Project.

The first transpose AMIP experiment is the control experiment which has a 3-month spin up period, followed by a year long simulation from January to December of 2013 with CO_2 concentrations of 348 ppm. This concentration is representative of the end of the twentieth century (AMIP period).

The second experiment consists of a 92-member ensemble of 30-day simulations initialized at midnight from every day of June-July-August (JJA) 2013 of the control experiment with CO_2 concentrations abruptly quadrupled. By initializing from different start dates, the noise due to weather is reduced. This experiment setup is similar to, but much shorter than, the CMIP6 *amip4xCO2* (Eyring et al., 2016) and will be denoted as Global4xCO$_2$ hereafter.

The third experiment similarly consists of 92 member of 30-day simulations, where, however, CO_2 concentrations are quadrupled only within the central European region and kept fixed at the reference concentration elsewhere on the globe. This will be denoted as Local4xCO$_2$ hereafter.

3. Shortwave Cloud Adjustments in CMIP5 Models

To determine whether the mean and variability of rapid cloud adjustments over central Europe is representative of that which we find globally, we make use of the fixed SST method (Forster et al., 2016) combined with the linearized radiative kernel technique (Shell et al., 2008). As noted above, this method takes cloud masking effects into account.

Figure 1 shows the multimodel mean and standard deviation of the CMIP5 models' rapid cloud adjustment. Globally, the multimodel mean is positive, as also reported by, for example, Zelinka et al. (2013) and Vial et al. (2013). Over land, the rapid cloud adjustments are more pronounced as the surface temperatures react on much faster timescale than over the ocean (Boucher et al., 2013). In particular, a strong positive rapid cloud adjustment is found over central Europe, North and South America, and Russia.
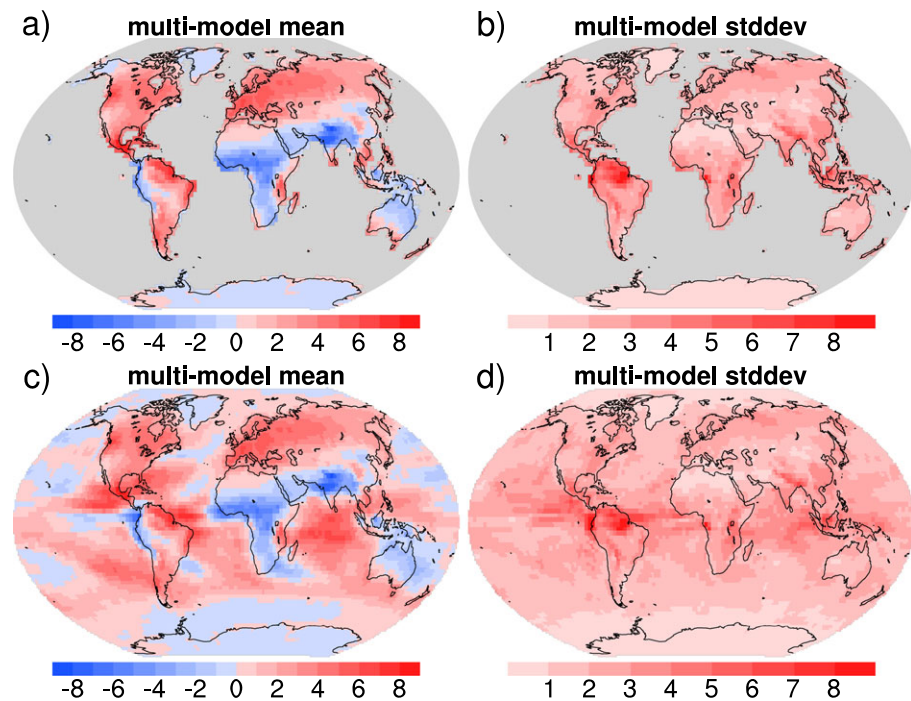
Figure 1. CMIP5 multimodel mean and standard deviation of rapid shortwave cloud adjustment (W/m^2) for (a, b) land only and (c, d) land and ocean based on the CMIP5 sstClim and sstClim4xCO2 experiments and radiative kernels of Shell et al., 2008 for 13 CMIP5 models. CMIP5 = 5th Coupled Model Intercomparison Project.
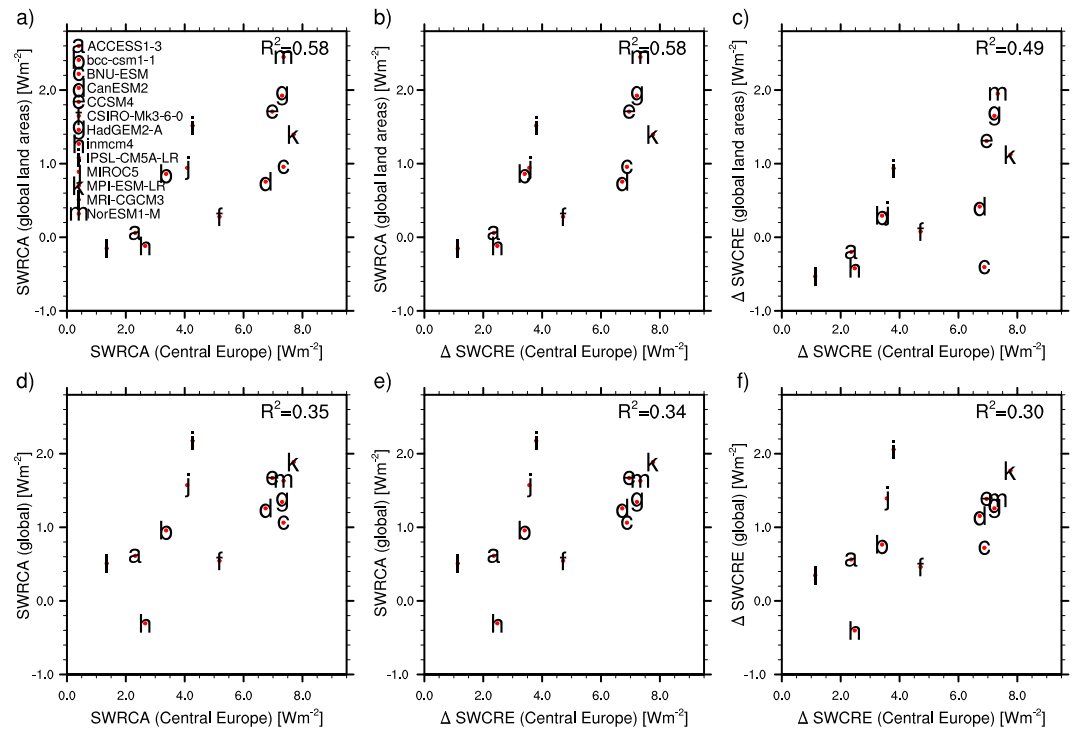
Figure 2. Area-averaged rapid shortwave cloud adjustments (SWRCAs) and difference of the shortwave cloud radiative effect (ΔSWCRE) for the sstClim4xCO2 minus the sstClim experiment from 13 5th Coupled Model Intercomparison Project models over central Europe (*x* axis) and (a–c) over global land areas (*y* axis) and (d–f) over global land and ocean (*y* axis).

Over central Europe, the multimodel mean of rapid cloud adjustments is ~5 W/m^2 with a standard deviation of ~2 W/m^2, indicating that rapid cloud adjustments over central Europe are variable and uncertain. In Figure 2a, the area-averaged shortwave component of the rapid cloud adjustments (SWRCAs) over the entire global land areas is plotted against that of the Central-European domain. We also analyze the relationship of the difference in shortwave cloud radiative effects between the abrupt4xCO2 and the Control run ΔSWCRE in central Europe and SWRCA based on the CMIP5 model output (Figure 2b) because in the following ICON-A GCM study ΔSWCRE is analyzed instead of SWRCA and used as a proxy for SWRCA which unlike ΔSWCRE accounts for cloud masking effects and removes contributions due to noncloud changes. We find that models with a higher SWRCA (or ΔSWCRE) over central Europe tend to have a higher response over the global land areas. The values, however, are smaller when averaging over all land areas compared to averaging just over central Europe (Figures 2a–2c). When the analysis is limited to JJA (Figure S1 in the supporting information), the R^2 is slightly smaller (0.55 in Figure S1a instead of 0.58 in Figure 2a), but the overall result is similar. Furthermore, in general, SWCRA and ΔSWCRE over central Europe are closely related (Figure S2). This is expected since albedo and water vapor changes exert less of an influence such as in polar regions or the tropics. The correlation of ΔSWCRE in central Europe with ΔSWCRE for global land areas in Figure 2c is slightly weaker than the correlation with SWRCA for global land areas in Figure 2b, and Figure S1c suggests that it also depends on the season. Correlations between central Europe and global land and ocean areas (Figures 2d–2f) are generally weaker, which might in part be due to the fact that SSTs are kept fixed while land surface temperatures are allowed to change. The relationship between SWRCA and changes of land surface temperature over central Europe is shown in Figure S3. The R^2 is for this relationship is 0.55.

In order to investigate how representative the SWRCA in central Europe is for the SWRCA over global land areas in different dynamical regimes as represented by the 500-hPa vertical pressure velocity ω_{500}, we repeated the analysis presented in Figure 2a for 12 ω_{500} bins from −120 hPa/day (strong ascent) to 120 hPa/day (strong descent), again based on monthly mean model output. The result is summarized in Figures 3a and 3b. Correlation plots for the individual bins are shown in Figure S4. The average ω_{500} for central Europe from the sstClim and sstClim4xCO2 experiments is close to 0 hPa/day (−0.004 hPa/day), and the highest R^2 in Figure 3b
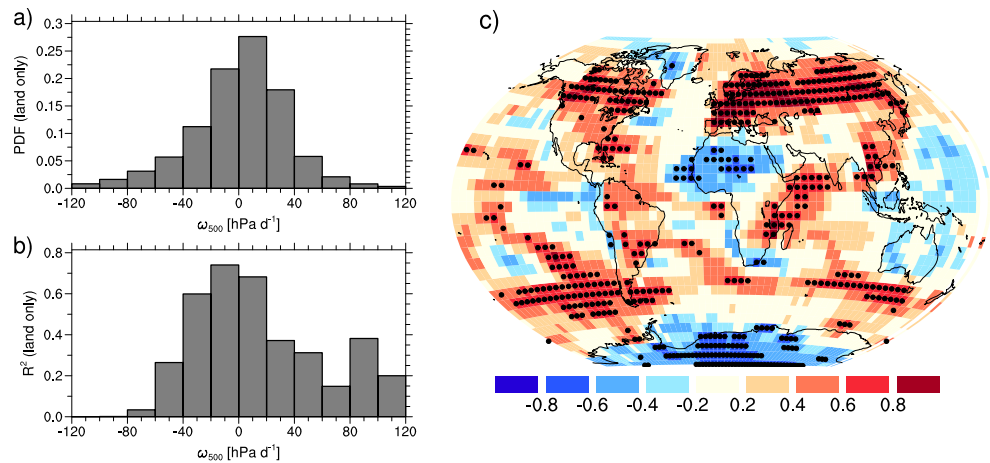
Figure 3. (a) Probability density function (PDF) of the monthly mean vertical pressure velocity at 500 hPa (ω_{500}) over global land areas in the 5th Coupled Model Intercomparison Project sstClim and sstClim4xCO2 experiments and (b) squared Pearson correlation coefficient (R^2) of SWRCA over central Europe and SWRCA over global land areas for 12 *dynamical regimes* represented by ω_{500} bins. (c) Pearson correlation coefficient (R) for SWRCA over central Europe and SWRCA over global land and ocean for $5° \times 5°$ grid boxes. Dots indicate grid points where the correlation is significant at the 95% level (using a Fisher *z* transformation). SWRCA = area-averaged shortwave component of the rapid cloud adjustment.

are found around 0 hPa/day, that is, in land regions with weak or moderate ascent and regions with weak descent, which are dynamically similar to central Europe. For regions with strong average ascent such as the intertropical convergence zone, and especially the Indian and African monsoon region (see Figure 3c), the correlation breaks down. If ocean regions are included in this analysis, the correlations are once again weaker (Figures S5 and S6). While over most global land areas, the SWRCA is positively correlated with the SWRCA over central Europe (Figure 3c); it should be noted that also negative correlations over some areas such as the Sahara, Greenland, and Antarctica (Figure 3c) result in a positive R^2.

In summary, the above analysis suggests (a) that ΔSWCRE over central Europe can be used as a proxy for SWRCA (in the absence of snow cover) and (b) that SWRCA over central Europe is representative of SWRCA over many global land areas. This latter finding implies that a constraint over central Europe, such as the one from a reference large-eddy simulation, may indeed be instructive for studying the processes influencing rapid cloud adjustments.

4. Shortwave Cloud Adjustments in the ICON-A GCM

4.1. Global and Local Cloud Radiative Effects

Having demonstrated that shortwave rapid cloud adjustments among CMIP5 models are highly variable, and over central Europe in particular, we will now demonstrate that this holds true for the new ICON-A GCM. We will also show that using present-day boundary conditions do not influence the shortwave cloud radiative adjustments for lead times less than 36 hr, thus suggesting that large-eddy simulations will prove useful for understanding the processes influencing for shortwave cloud adjustments, for example, convective mixing, turbulence, or stability.

It should be noted in the following section that we analyze the changes to the radiative budget on very short terms, on the order of a few days, which is a realistic duration for large-eddy simulations. As such, *shortwave rapid cloud adjustment* in this case is simply the change in top-of-atmosphere shortwave cloud radiative effects. This differs from the classical definition of shortwave rapid cloud adjustments in which the contributions from water vapor and albedo are removed using radiative kernels (Shell et al., 2008), then regressed to find the *y* intercept (Gregory et al., 2004). We argue that given the location, season, and timescale which we are considering, the changes to shortwave cloud radiative effects should be less sensitive to water vapor and albedo forcings. As demonstrated above, for this location the use of shortwave cloud radiative effects is not an issue for the purpose of this paper, which is to determine whether large-eddy simulations may in principle be used as a reference to constrain rapid cloud adjustments in GCMs.
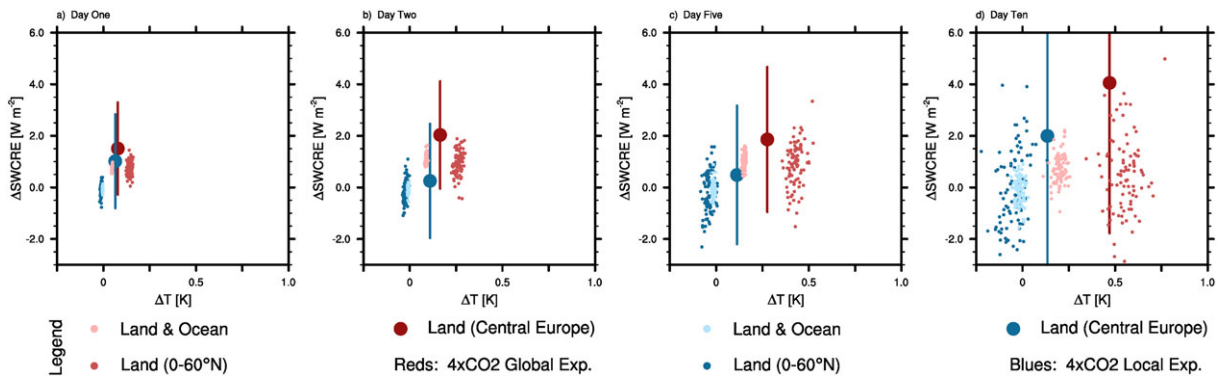
Figure 4. Shortwave cloud radiative effective at top-of-atmosphere (ΔSWCRE) on Days (a) 1, (b) 2, (c) 5, and (d) 10. Differences calculated from Global $4xCO_2$-AMIP experiments in red, and Local $4xCO_2$-AMIP experiments in blue. Bars span the standard error of the mean. AMIP = Atmospheric Model Intercomparison Project.

The plots within Figure 4 are structured such that differences in the shortwave radiation budget at top-of-atmosphere due to clouds, (ΔSWCRE), is plotted against the change in surface temperature ΔT_s for days 1, 2, 5, and 10 after the abrupt change in CO_2 concentration, similar to the works of Dong et al. (2009) and Bony et al. (2013). These selected days present a snap shot of the three phases defined by Dong et al. (2009): immediate response of troposphere and surface processes (Day 1), rapid adjustment of surface processes (Days 2–5), and tropospheric adjustment (Day 6 onward). In Figure 4 the daily average of the differences between the perturbed $4xCO_2$ and AMIP experiments, for each ensemble member, is presented by a small dot. Red colors denote the *Global 4xCO2* experiments, whereby blue colors denote the *Local 4xCO2* experiments. Light colors indicate global values, which are calculated from land and ocean grid points, whereas the dark colors indicate land-only values of the NH between 0 and 60°N. We focus on the NH land points because of the difference in hemispheric warming during the JJA period. The large dots are the 92-member ensemble mean, with bars spanning the standard error of the mean, of ΔSWCRE over central Europe. The ensemble mean over central Europe is presented because there are only 39 grid points over central Europe per ensemble member and changes of ± 110 W/m^2 are possible, although the majority of the distribution is within ± 50 W/m^2 typically (not shown). This also suggests that for the ICON-LEM experiment, a large sample size will be necessary to eke out a statistically significant signal in changes in the radiative budget. Within these simulations of ICON-A GCM, 8.6×10^4 grid points go into the calculating the daily mean of ΔSWCRE. The variability is projected to decrease significantly with the ICON-LEM simulations with 1.0×10^{10} grid points going into the calculations of the daily mean. This is over 115,000 times more points. Our hypothesis is that the large number of grid points in the aforementioned large-domain LES perturbed CO_2 and control simulations will help to average out the noise. This hypothesis will be investigated when the large-eddy simulation is completed.

Focusing on Day 1 (Figure 4a), the small cluster of light red dots yields a mean ΔSWCRE of ~0.74 W/m^2 in the ICON-A GCM Global$4xCO_2$ experiment. The clear distinction between the small light and dark red dots shows that the land surface warms faster than the ocean and shows more variability among the ensemble members. The reduction of sample size by only considering land points also contributes to the spread in ensemble variability, but not significantly. Overlaying the cluster of light red dots are two large dots marking the central European means of the Global$4xCO_2$ and Local$4xCO_2$ experiments. The differences between their respective means, of 1.5 and 1.0 W/m^2, is evidence of the large-scale environment's influence on rapid shortwave cloud adjustments. Focusing on the Local$4xCO_2$ alone, the ΔSWCRE over central Europe is distinct from both the *land and ocean* as well as all *land-only* points of the NH. This is not surprising as there was no CO_2 forcing outside of central Europe.

The ability of the Local$4xCO_2$ experiment to produce values of ΔSWCRE from the Global$4xCO_2$, as seen from the mean and standard error of the mean, shows that a local perturbation experiment is representative of global perturbations on Day 1. This implies that the ΔSWCRE calculated from a $4xCO_2$ ICON-LEM experiment ought to be representative too; despite being driven with present-day meteorological conditions at the boundaries (i.e., $1xCO_2$ concentrations outside the model domain). This is an important result for the overarching aim of this study.

In both the Global4xCO$_2$ and Local4xCO$_2$, the ΔSWCRE becomes more variable over time, especially over land. On Days 2 through 10, the difference in daily mean between the Local4xCO$_2$ and Global4xCO$_2$ ΔSWCRE, over central Europe, is 2 W/m^2, which is far less than the 7 W/m^2 spread among the CMIP5 models (see Figure 2). The changes in surface temperature (ΔT) also increase with time, leading to increasing differences between the central European ensemble means, and their standard error of mean ranges, of the two experiments. This is expected since advection, circulation changes, and increasingly strong land surface temperature increases become increasingly more relevant. On Days 1 and 2, the central European surface temperature of the Local4xCO$_2$ and Global4xCO$_2$ experiments are very similar. On Day 5 the surface temperature has increased much more for the Global4xCO$_2$ than the Local4xCO$_2$ experiment, with differences reaching ~0.3 K by Day 10. The standard error of ΔSWCRE over central Europe, on Day 10, approximately spans 8 to -4 W/m^2 for the Global4xCO$_2$ compared to 10 to -2 W/m^2 in the Local4xCO$_2$ experiment. One can see that with longer integration times, certainly by Day 10, advection and circulation plays an increasingly large role and a local perturbation is not representative anymore. Figure 4 shows that the standard error of the mean ΔSWCRE over central Europe, up until Day 5, are less than the spread of CMIP5 models. Until Day 5, the spread among the ΔSWCRE means of the NH global land points are comparable with the variability found among the CMIP5 models. In the next section, we look more closely at the time series of ΔSWCRE as well as other properties.

4.2. Cloud Radiative Effects: Time Series

A time series of the changes to ensemble mean in $\Delta NetCRE$ over central Europe for the first 5 days is presented in Figure 5a. Alongside it are its shortwave and longwave components, the surface temperature, and sensible and latent surface heat fluxes. Red lines indicate the Global4xCO$_2$ experiment, whereas blue lines are the Local4xCO$_2$ experiment. The shaded regions are the standard deviation of the ensemble differences between the perturbed and AMIP experiment at each time step. The time series presented in Figure 5 allow us to determine extent which the changes found in the Local4xCO$_2$ experiment are representative of Global4xCO$_2$ in terms of magnitude, variability, and temporal duration.

The most striking feature among the plots in Figure 5 is the strong diurnal cycle. The greatest differences in $\Delta NetCRE$ (Figure 5a) occur around noon in both Global4xCO$_2$ and Local4xCO$_2$ experiments. A comparison of the shortwave (ΔSWCRE) and longwave (ΔLWCRE) components show that the shortwave component contributes more to the strength and variability seen in the $\Delta NetCRE$, right from the start. Both experiments show a ΔSWCRE of at least 2 W/m^2 over the period of a day. The ΔLWCRE component of the two experiments is nearly identical for the first 5 days and shows relatively little variability compared to the ΔSWCRE. One should exercise caution should one wish to draw conclusions from the ΔLWCRE regarding rapid cloud adjustments, as the contributions from the CO$_2$, water vapor, atmospheric temperature, surface temperature, and ongoing stratospheric adjustment would need to be removed; all of which are nonnegligible (Shell et al., 2008; Zhang & Huang, 2014).

The ΔT of the two perturbed experiments in Figure 5d are nearly identical and have the same magnitude of variability over the first ~36 hr of the simulations. In the first 24 hr, the two experiments show a surface temperature increase of 0.1 K, peaking at noon, and growing to 0.2 K on the second day. After 36 hr the changes in ΔT over central Europe diverge between the two experiments, with Global4xCO$_2$ increasing with time, peaking on Day 8 and returning to 0.4 K on Day 10 similar to Dong et al. (2009; not shown).

Changes in the atmospheric radiation budget and surface temperature are vital to the sensible heat flux, latent heat flux, and surface heating, which in turn influences processes such as evaporation and resistance. Over land, the local sensible and latent heat fluxes have a critical role in the development of the boundary layer and convection. Dong et al. (2009), Doutriaux-Boucher et al. (2009) and Andrews and Ringer (2014) found that plant physiological forcing plays an important role in determining cloud adjustments in the HadAM3 and HadGEM2-ES climate models, respectively, due to the increasing surface temperature. The plants contributed to low-level cloud changes because of an increase in sensible heat flux and decrease in latent heat flux caused by stomatal closure. In the simulations analyzed here, no interactive vegetation is considered, so this particular response is not included. Focusing on the first 36 hr, we see that the sensible heat flux fluctuates between ± 1 W/m^2 over the day while the latent heat flux increases by 3 W/m^2. Over the period of 10 days, the sensible heat transfer from the surface and latent heat flux from evaporation both increase in the two perturbed CO$_2$ experiments (not shown) resulting in increased transport of heat and moisture from the surface to the atmosphere, particularly the boundary layer.
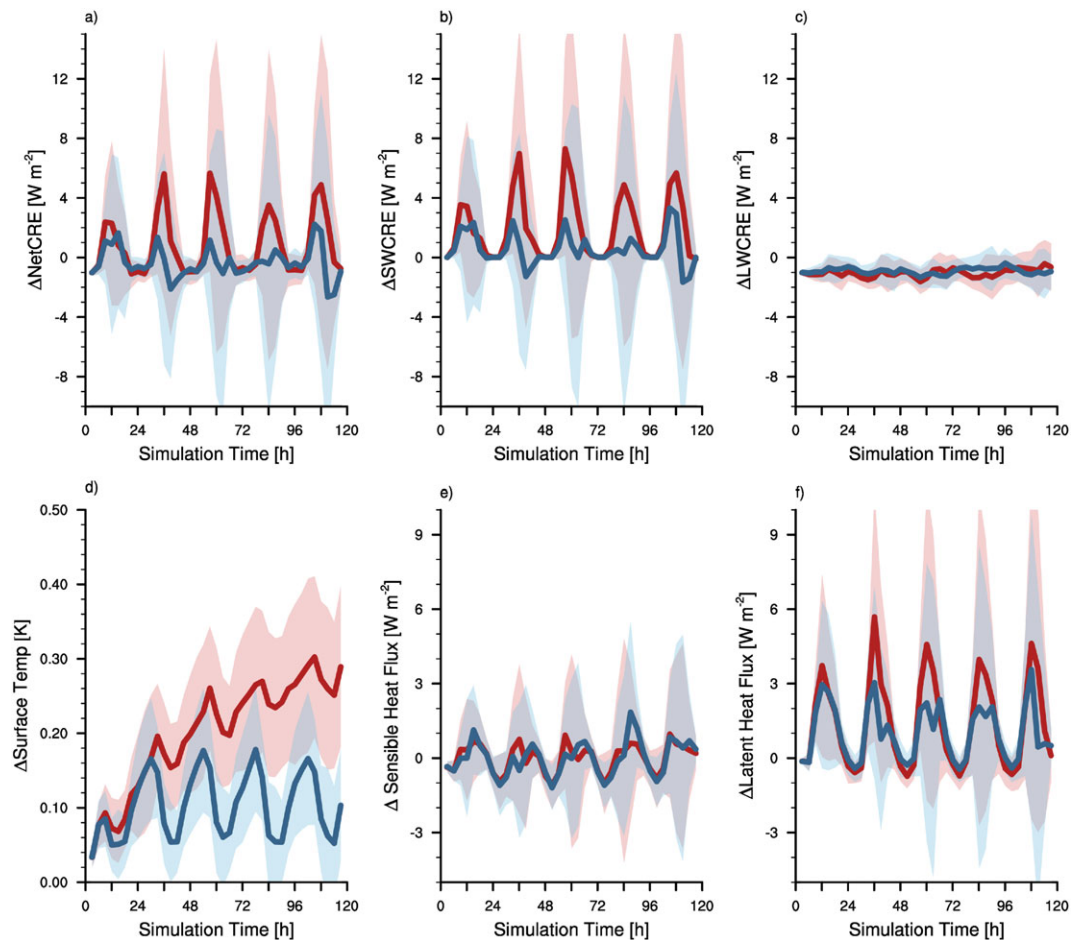
Figure 5. Time series from Days 1 to 5 over central European domain for (a) net cloud radiative effect (CRE) at top of atmosphere, (b) shortwave component of CRE (SWCRE), (c) longwave component of CRE (LWCRE), (d) surface temperature, (e) surface sensible heat flux, and (f) surface latent heat flux. Thick red and blue lines denote 92-member ensemble mean of the differences between Global 4xCO$_2$-AMIP experiments (red), and Local 4xCO$_2$-AMIP experiments (blue). Shaded areas denote the standard deviation of the ensemble differences. AMIP = Atmospheric Model Intercomparison Project.

All in all, the Local4xCO$_2$ experiment captures changes with time of the Global4xCO$_2$ experiment, in terms of magnitude and variability, in the first approximately 36 hr after the perturbation. The similar time series of the two perturbed experiments in Figure 5 suggests that the ICON-LEM perturbed-CO$_2$ simulation will be able to capture changes in atmospheric radiative warming, surface temperature, and thereby the changes to surface fluxes, for up to 2 days. The time series also shows that the large-scale environment is not of significant relevance for the first 36 hr for these variables.

4.3. Tropospheric Profiles of Central Europe

Dong et al. (2009) had concluded that abrupt changes in tropospheric radiative heating could alter local lapse rates and the stability, affecting convection and clouds, and thereby the top-of-atmosphere radiation budget. As such we consider vertical profiles of tropospheric specific humidity, RH, potential temperature, cloud fraction, cloud liquid water content, and cloud ice water content on Day 2, from 9 to 15 hr, where the changes in the Local4xCO$_2$ experiment still resemble Global4xCO$_2$ (Figure 6). The differences in the ensemble means, over central Europe, of the Local4xCO$_2$ and Global4xCO$_2$ experiments relative to the AMIP experiment are compared, in blue and red, respectively, and the shaded regions denote the standard error of the mean for each level. It should be noted that the differences between the mean abrupt4xCO$_2$ and AMIP tropospheric profiles taken at 12 hr on Days 1 through 5 are nearly identical as those seen in Figure 6 and as such are not presented. The statements below are written such that they also hold for both Day 2 and Days 1 to 5 unless otherwise stated.
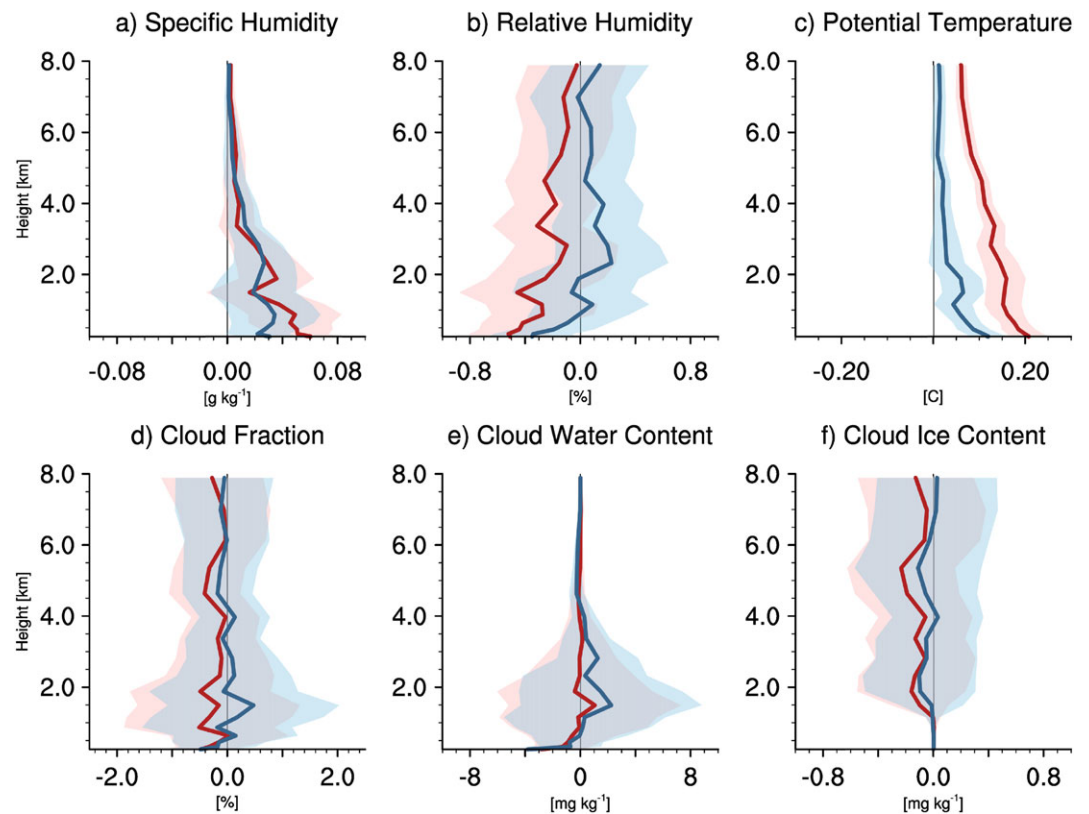
Figure 6. Difference plots of 92-member ensemble mean atmospheric profiles of the troposphere over central Europe on Day 2 from 9 to 15 hr: Global4xCO$_2$-AMIP (red), and Local4xCO$_2$-AMIP (blue). Shaded areas denote the standard error of the mean. AMIP = Atmospheric Model Intercomparison Project.

As expected with the increase in latent heat flux at the surface, the vertical profiles of specific humidity, in Figure 6a, show a maximum difference of 0.03 g/kg in the lowest 1 km, and decreasing until all three experiments are nearly identical upward of 4 km. The changes in the Local4xCO$_2$ are weaker than that of the Global4xCO$_2$ experiment, although the two distributions overlap. Changes in RH profiles, in Figure 6b, are similar in structure; however, the Global4xCO$_2$ experiment shows a definite decrease in RH throughout the troposphere, particularly in the lower troposphere (<4 km). In comparison, the RH profiles in the Local4xCO$_2$ experiment only shows a decrease below 1 km. The decrease in RH can be attributed to a slight increase in potential temperature of 0.2°C in the Global4xCO$_2$ experiment, and 0.1°C in the Local4xCO$_2$ experiment, combined with a weaker increase in specific humidity. The differences in potential temperature, in Figure 6c, are greatest near the surface, and the profiles of Local4xCO$_2$ are nearly identical to the AMIP experiment above the lowest 2 km. The changes in the Local4xCO$_2$ experiment are much weaker than the Global4xCO$_2$ experiment, and while they appear to have the same magnitude of variability, they do not overlap. The differences in potential temperature are greater for the Days 1-to-5 study, where the differences in potential temperature in the upper troposphere grow to ~0.15°C, while the surface remains near ~0.2°C, in the Global4xCO$_2$ experiment.

In terms of cloud fraction (Figure 6d), the ICON-A GCM shows very little change, less than ±1%, in the ensemble mean. In both the Local4xCO$_2$ and Global4xCO$_2$ experiments, there is a slight decrease in cloud fractions in the lowest model layers which is also seen in the profile of cloud liquid water. The cloud liquid water in, in Figure 6e, the Global4xCO$_2$ experiment shows little change except near the surface; however, the Local4xCO$_2$ shows a more complicated picture with the decrease near the surface and increase between 1 and 3 km. The decrease in cloud liquid water in the Global4xCO$_2$ experiment becomes more evident in the Days 1-to-5 analysis, while the Local4xCO$_2$ still shows a decrease below 1 km and increase above 1 km. The cloud ice water profiles in Figure 6f show a more consistent picture with a slight decrease throughout the troposphere in the two perturbed experiments. The lower three panels of Figure 6 show large variability among the cloud properties, which is captured by the Local4xCO$_2$ experiment.

After an abrupt change in CO_2 concentration, the reduction in RH in the lower troposphere, and slight decrease in cloud fraction near the surface due to temperature changes, is qualitatively consistent with other modeling studies, such as Kamae and Watanabe (2012) and Colman and McAvaney (2011), even for this limited domain. The changes associated with rapid cloud adjustments to thermodynamic properties and clouds produced by the Global4xCO_2 are captured by the Local4xCO_2 experiment. The discrepancies seen in the lowest 2 km motivates the use of an LEM study as they can resolve the evolution of the boundary layer better.

4.4. Convective Mixing Index Over Central Europe

Given the large variability in changes in cloud fraction, we strive to better understand the changes in terms of a physical mechanism that one can assess in both the ICON-A GCM and ICON-LEM. Here we consider the convective mixing index, μ (equation (1)), first proposed by Vial et al. (2016), which measures the strength of convective transport of moist static energy (MSE) in the lower troposphere. Vial et al., 2016 demonstrated that a stronger convective mixing index over the marine boundary layer leads to a reduction of low-level cloud fraction. It has also been shown by Sherwood et al., 2014 that the strength of convective mixing in GCMs determines the rate in which the low-cloud layer is dehydrated and the strength of the convective mixing explains half of the variance in climate sensitivity projections.

$$\mu = \int_{p_1}^{p_{top}} \left(-\partial_p \overline{\omega'h'} \mid_{con} \right) \frac{dp}{g} - \int_{p_0}^{p_1} \left(-\partial_p \overline{\omega'h'} \mid_{con} \right) \frac{dp}{g}$$
$$= 2\overline{\omega'h'} \mid_{con} (p_1)$$

(1)

The convective mixing index of Vial et al., 2016, was originally developed to study the marine boundary layer in the single-column Laboratoire de Météorologie Dynamique (IPSL-CM5A-LR) model and as such, we have made one minor adjustment to equation (1). The terms of equation (1) are defined as follows: $-\partial_p \overline{\omega'h'} \mid_{con}$ denotes the vertical convergence of the MSE flux due to convection (computed from model tendencies), p_0 is the pressure of the lowest model level, p_1 is the model level where the upward convective flux of MSE is maximum, and p_{top} is the pressure at the top of the marine boundary layer. We have computed the convective mixing index for the central European domain on Day 2 from 9 to 15 hr, as in section 4.3; however, we have extended p_{top} from ~ 750 to 650 hPa in our calculations. Seidel et al., 2012 shows that the boundary layer top over Europe in the months of JJA the boundary layer top, when defined by the bulk Richardson number with a critical value of 0.25, exceeds 2 km in 10% of the Integrated Global Radiosonde Archive radiosondes (Durre & Yin, 2008) as well as ERA-Interim reanalysis of the European Centre for Medium-Range Weather Forecasting (Dee et al., 2011).

Due to limited computational resources, the convective tendencies of only one member of the 92-member ensemble has been used in the computation of the convective mixing index. The convective tendencies of temperature and humidity were used to calculate the convective contribution to MSE, whose mean profiles are shown in Figure 7a. The profiles show that in both the Local4xCO_2 and Global4xCO_2 experiments, the maximum MSE tendency due to convection is reached at lower altitudes and strengthens; reflecting the change in RH profiles shown in Figure 6b as convection, both shallow and deep, tends to dry the lowest layers of the troposphere.

From the profiles of MSE tendency due to convection, the level of maximum upward MSE flux is identified as p_1 from which we calculate μ being equal to twice the maximum upward flux of MSE at (second line of equation (1). In Figure 7b, the convective mixing index of the Local4xCO_2 and Global4xCO_2 simulations are compared with the black line denoting the regression of μ over central Europe along with the corresponding squared Pearson correlation coefficient (R^2) after the removal of two statistical outliers in the Global4xCO_2 simulations. We see that the convective mixing index of the Global4xCO_2 and Local4xCO_2, and their changes (Figure 7c), show a very weak positive correlation over central Europe, with an R^2 of 0.15 and 0.16, respectively. The strength of $\Delta\mu$ in the two abrupt4xCO2 experiments are negatively correlated with the strength of μ in the AMIP experiments with an R^2 of 0.27 over central Europe (not shown).

Despite the convective mixing index capturing the drying of troposphere's lowest layers, we do not see a correlation between the change in convective mixing and cloud cover (not shown), nor ΔSWCRE (Figure 7d). This is likely due to the fact the convective mixing index does not account for the possibility of increased cloud cover aloft as well as non-re-evaporating precipitation playing a greater role over land relative to the marine boundary layer as in the work of Vial et al. (2016). It would be of interest in the ICON-LEM paper to repeat
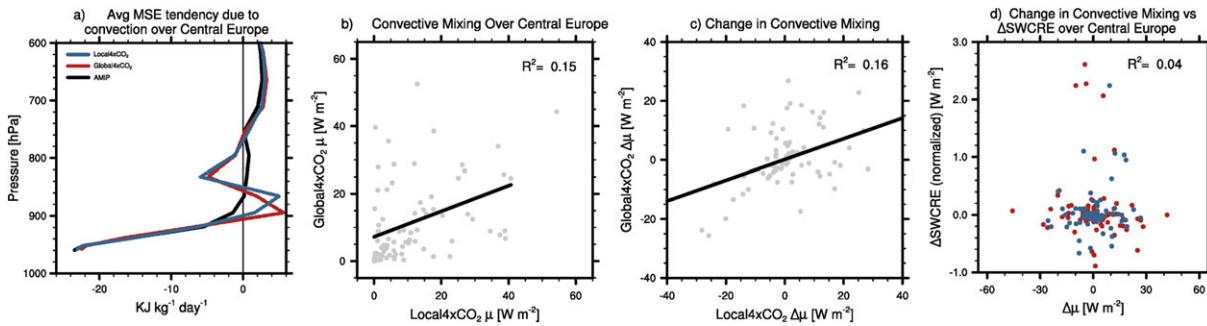
Figure 7. Day 2 from 9 to 15 hr over central Europe: (a) Mean moist static energy (MSE) tendencies due to convection for AMIP in black, Local4xCO$_2$ in blue, and Global4xCO$_2$ in red; (b) scatter plots of the convective mixing index (μ) of Global4xCO$_2$ and Local4xCO$_2$; (c) changes in convective mixing index ($\Delta\mu$) for the abrupt4xCO$_2$-AMIP experiments versus the convective mixing index (μ) of AMIP; and (d) changes in ΔSWCRE relative to $\Delta\mu$. Black lines denote the regression lines of the abrupt4xCO$_2$ experiments over central Europe. The corresponding squared Pearson correlation coefficients (R^2) are also presented. AMIP = Atmospheric Model Intercomparison Project; SWCRE = shortwave cloud radiative effect.

this experiment with a larger ensemble in order to be able to filter out higher-level clouds and identify changes to only low-level clouds, as well as sample across different large-scale conditions.

In this section we attempted to identify an index to which the changes in ΔSWCRE could be tied to a process that could also be diagnosed in the ICON-LEM. Using the convective mixing index of Vial et al., 2016, we, unfortunately, do not find a correlation among μ and ΔSWCRE in our small sample over central Europe due to little change in total cloud cover. The convective mixing index appears to capture the drying of the boundary layer.

5. Limitations

The overarching question of this paper is to determine whether a single short, high-resolution ICON-LEM regional simulation can serve as a proxy for assessing and constraining rapid cloud adjustments to an instantaneous quadrupling of CO$_2$ in global atmospheric models. In this work we have identified and addressed four major differences between the proposed ICON-LEM configuration and the existing GCM configuration (e.g., CMIP5 sstClim4xCO2), which need to be accounted for: diagnosed variable, ensemble size, area of perturbation, and timescale of evaluation (Table 2).

There are, however, two important limitations of the current study: (i) the first is that a short LEM simulation will only capture a single weather regime, which may not be representative of the overall climate impact; and (ii) the second is that a short deterministic LEM simulation cannot capture circulation changes.

In regard to determining whether the ΔSWCRE in a single ICON-LEM simulation, which is influenced by the initial synoptic regime, is representative of the ΔSWCRE of the ICON-A GCM and other CMIP5 models, which represents the statistical mean across synoptic regimes, we recommend for future work to consider performing a cluster analysis on the three indices's of synoptic-scale flow, which are geostrophic flow strength, vorticity, and direction (Osborn et al., 1999) or by weather regimes.

Table 2
Difference Between ICON-LEM, ICON-GCM, and CMIP5 Configuration

Difference	ICON-LEM	ICON-GCM	CMIP5 sstClim4xCO$_2$
Diagnostic (section 3)	ΔSWCRE	ΔSWCRE and SWRCA	SWRCA
Ensemble size (section 4.1)	Single realization; 10^{10} grid points	92 member ensemble; short-term average; fewer points	Long-term average; fewer points
4xCO$_2$ perturbation (section 4.1)	Local (central Europe)	Local (central Europe) and Global	Global
Timescale (section 4.2)	<36 hr: immediate thermodynamic effects	Days: immediate thermodynamic effects and circulation response	Days to Months: immediate thermodynamic effects and circulation response

Note. ICON = Icosahedral Non-hydrostatic; LEM = large-eddy model; GCM = general circulation model; CMIP5 = 5th Coupled Model Intercomparison Project; SWCRE = shortwave cloud radiative effect; SWRCA = shortwave component of the rapid cloud adjustment.

In regard to the circulation changes, the CMIP5 sstClim4xCO$_2$ simulations include contributions from the large-scale dynamical (circulation) changes, which may need to be removed for a direct comparison with the immediate ΔSWCRE from ICON-LEM such that the short-term (e.g., Days 1–2) ΔSWCRE can be linked to the long-term (e.g., Day 10) ΔSWCRE (or SWRCA) in a meaningful way.

There is, however, no simple way of scaling between the short-term (Day 1) ΔSWCRE and the longer-term (Day 10) ΔSWCRE, because when attempting to correlate the SWCRE at Day 1 and Day 10 the weather *noise* overwhelms the signal. Nonetheless, it is still physically expected that the short-term effects entail, or bring about, the longer-term (Day 10) effect. The work presented here is founded on the idea that Day-1 effects are more uncertain across climate models, since parameterized physics are more relevant, compared to Day 10 effects that are more of a mesoscale circulation response, which is better described by the resolved model equations. Although in principle weather noise can be averaged out by averaging over large domains and longer timescales (as suggested, e.g., by the Figure S7 in the supporting information), this would require longer ICON-LEM runs with large domains. An alternative approach to reducing the impact of weather noise is to use a large ensemble initiated from different start dates. With respect to model initialization one could follow the method described in Ma et al. (2015).

Should one want to try decomposing the ΔSWCRE into local thermodynamic and large-scale dynamic components in the GCM simulations, using some measure of synoptic-scale flow based on geostrophic flow strength, vorticity, and direction (Osborn et al., 1999), it may be possible to apply the ICON-LEM constraint to the local component alone. In addition, the measure of synoptic-scale flow could be used to quantify the statistical representativeness of the large-scale environment of the ICON-LEM simulation.

Despite these two limitations, the authors believe these first results suggest that a regional ICON-LEM simulation could be instructive for assessing and constraining global rapid cloud adjustments.

6. Conclusion

This study was designed to determine whether large-eddy simulations may, in principle, be used to constrain rapid shortwave cloud adjustments in GCMs despite the fact that LEMs can only be run on over limited area, for a short period of time, and are influenced by boundary conditions.

The origin of diversity in rapid cloud adjustments, as shown by Vial et al. (2013) and Zelinka et al. (2013), has been attributed to the low clouds, in particular the optically thick ones, that strongly influence the shortwave cloud radiative effects. As such we first determined that both changes in shortwave rapid cloud adjustments, and in shortwave cloud radiative effects, over central Europe behave qualitatively similarly as over global land areas in a CMIP5 multimodel ensemble.

Through the combination of three transpose AMIP-style experiments, we investigated the extent to which changes in rapid shortwave cloud adjustments calculated from a CO$_2$ perturbation contained over central Europe, was representative of those calculated from a global 4xCO$_2$ perturbation using the new ICON-A GCM.

From the ensemble of $\Delta NetCRE$, as analyzed in the ICON-A simulations showed that the strength and spread of $\Delta NetCRE$ are largely determined by the SW component. We found that a clear signal in the net top-of-atmosphere SW cloud radiative effect emerges after an abrupt4xCO$_2$ perturbation and that for timescales less than ~36 hr, rapid shortwave cloud adjustments on a local scale are representative, in terms of mean and variability, of the global scale. Beyond that, advection and circulation cause the Local4xCO$_2$ and Global4xCO$_2$ ensemble means to diverge.

A comparison of vertical profiles over central Europe showed the Local4xCO$_2$ produced similar changes to the thermodynamic and cloud properties as the Global4xCO$_2$ experiment in the new ICON-A GCM model. Together these results showed that atmospheric processes related to rapid shortwave cloud adjustments over central Europe are largely a local, thermodynamically driven phenomenon, and rather independent of larger-scale dynamical effects on short timescales less than 2 days. Lastly, we computed the convective mixing index, which showed a very weak positive correlation between the abrupt4xCO$_2$ experiments over central Europe.

Together these results suggest that a LEM perturbed with 4xCO$_2$, over central Europe, ought to be instructive for learning how rapid shortwave cloud adjustments manifest and ultimately help with constraining

rapid shortwave cloud adjustments, and climate sensitivity, in GCMs, despite being driven with present-day meteorology at its boundaries, when performed with a sufficiently large resolution and for a short period of time.

From the result of this work, we recommend that the ICON-LEM simulations, which have begun as part of the German-wide research initiative *High-Definition Clouds and Precipitation for Climate Prediction* ($HD[CP]^2$) project, be run for at least 36 hr.

References

Andrews, T., & Forster, P. M. (2008). CO_2 forcing induces semi-direct effects with consequences for climate feedback interpretations. *Geophysical Research Letters*, *27*, L0480. https://doi.org/10.1175/JCLI-D-13-00421.1

Andrews, T., Gregory, J. M., Forster, P. M., & Webb, M. J. (2012). Cloud adjustment and its role in CO_2 radiative forcing and climate sensitivity: A review. *Surveys in Geophysics*, *33*, 619–635. https://doi.org/10.1007/s10712-011-9152-0

Andrews, T., & Ringer, M. (2014). Cloud feedbacks, rapid adjustments, and the forcing-response relationship in a transient CO_2 reversibility scenario. *Journal of Climate*, *27*, 1799–1818. https://doi.org/10.1175/JCLI-D-13-00421.1

Arora, V. K., Scinocca, J. F., Boer, G. J., Christian, J. R., Denman, K. L., Flato, G. M., et al. (2011). Carbon emission limits required to satisfy future representative concentration pathways of greenhouse gases. *Geophysical Research Letters*, *38*, L05805. https://doi.org/10.1029/2010GL046270

Bentsen, M., Bethke, I., Debernard, J. B., Iversen, T., Kirkevåg, A., Seland, Ø., et al. (2013). The Norwegian Earth System Model, NorESM1-M—Part 1: Description and basic evaluation of the physical climate. *Geoscientific Model Development*, *6*, 687–720. https://doi.org/10.5194/gmd-6-687-2013

Bi, D., Dix, M., Marsland, S., O'Farrell, S., Rashid, H., Uotila, P., et al. (2013). The ACCESS coupled model: Description, control climate and evaluation. *Australian Meteorological and Oceanographic Journal*, *63*, 41–64.

Block, K., & Mauritsen, T. (2013). Forcing and feedback in the MPI-ESM-LR coupled model under abruptly quadrupled CO_2. *Nature Geoscience*, *6*, 447–451. https://doi.org/10.1038/ngeo1799

Blossey, P. N., Bretherton, C. S., Cheng, A., Endo, S., Heus, T., Lock, A. P., & van der Dussen, J. J. (2016). CGILS Phase 2 LES intercomparison of response of subtropical marine low cloud regimes to CO_2 quadrupling and a CMIP3 composite forcing change. *Journal of Advances in Modeling Earth Systems*, *8*, 1714–1726. https://doi.org/10.1002/2016MS000765

Bony, S., Bellon, G., Klocke, D., Sherwood, S., Fermepin, S., & Denvil, S. (2013). Robust direct effect of carbon dioxide on tropical circulation and regional precipitation. *Nature Geoscience*, *6*, 447–451. https://doi.org/10.1038/ngeo1799

Boucher, O., Randall, D., Artaxo, P., Bretherton, C., Feingold, G., Forster, P., et al. (2013). Clouds and aerosols. In T. F. Stocker, D. Qin, G.-K. Plattner, M. Tignor, S. K. Allen, J. Boschung, et al. (Eds.), *Climate Change 2013: The Physical Science Basis. Contribution of Working Group I to the Fifth Assessment Report of the Intergovernmental Panel on Climate Change*. Cambridge, UK and New York: Cambridge University Press.

Cess, R. D., & Potter, G. L. (1988). A methodology for understanding and intercomparing atmospheric climate feedback processes in general circulation models. *Journal of Geophysical Research*, *93*, 8305–8314. https://doi.org/10.1029/JD093iD07p08305

Colman, R. A., & McAvaney, B. J. (2011). On tropospheric adjustment to forcing and climate feedbacks. *Climate Dynamics*, *36*, 1649–1658. https://doi.org/10.1007/s00382-011-1067-4

Dee, D. P., Uppala, S. M., Simmons, A. J., Berrisford, P., Poli, P., Kobayashi, S., et al. (2011). The ERA-Interim reanalysis: Configuration and performance of the data assimilation system. *Quarterly Journal of the Royal Meteorological Society*, *137*, 553–597. https://doi.org/10.1002/qj.828

Dong, B., Gregory, J., & Sutton, R. (2009). Understanding land-sea warming contrast in response to increasing greenhouse gases. Part I: Transient adjustment. *Journal of Climate*, *22*, 3079–3097. https://doi.org/10.1175/2009JCLI2652.1

Doutriaux-Boucher, M., Webb, M. J., Gregory, J. M., & Boucher, O. (2009). Carbon dioxide induced stomatal closure increases radiative forcing via a rapid reduction in low cloud. *Geophysical Research Letters*, *36*, L02703. https://doi.org/10.1029/2008GL036273

Dufresne, J.-L., Foujols, M.-A., Denvil, S., Caubel, A., Marti, O., Aumont, O., et al. (2013). Climate change projections using the IPSL-CM5 Earth system model: From CMIP3 to CMIP5. *Climate Dynamics*, *40*, 2123–2165. https://doi.org/10.1007/s00382-012-1636-1

Durre, I., & Yin, X. (2008). Enhanced radiosonde data for studies of vertical structure. *Bulletin of the American Meteorological Society*, *89*, 1257–1262. https://doi.org/10.1175/2008BAMS2603

Eyring, V., Bony, S., Meehl, G. A., Senior, C. A., Stevens, B., Stouffer, R. J., & Taylor, K. E. (2016). Overview of the Coupled Model Intercomparison Project Phase 6 (CMIP6) experimental design and organization. *Geoscientific Model Development*, *9*, 1937–1958. https://doi.org/10.5194/gmd-9-1937-2016

Forster, P. M., Richardson, T., Maycock, A. C., Smith, C. J., Samset, B. H., Myhre, G., et al. (2016). Recommendations for diagnosing effective radiative forcing from climate models for CMIP6. *Journal of Geophysical Research: Atmospheres*, *121*, 12,460–12,475. https://doi.org/10.1002/2016JD025320

Gent, P. R., Danabasoglu, G., Donner, L. J., Holland, M. M., Hunke, E. C., Jayne, S. R., et al. (2011). The community climate system model version 4. *Journal of Climate*, *24*, 4973–4991. https://doi.org/10.1175/2011JCLI4083.1

Giorgetta, M. A., Brokopf, R., Crueger, T., Esch, M., Fiedler, S., Helmert, J., et al. (2018). ICON-A, the atmosphere component of the ICON Earth system model. Part I: Model description. *Journal of Advances in Modeling Earth Systems*, *10*. https://doi.org/10.1029/2017MS001242

Giorgetta, M., Jungclaus, J., Reick, C. H., Legutke, S., Bader, J., Böttinger, M., et al. (2013). Climate and carbon cycle changes from 1850 to 2100 in MPI-ESM simulations for the Coupled Model Intercomparison Project phase 5. *Journal of Advances in Modeling Earth Systems*, *5*, 572–597. https://doi.org/10.1002/jame.20038

Gregory, J. M., Ingram, W. J., Palmer, M. A., Jones, G. S., Stott, P. A., Thorpe, R. B., et al. (2004). A new method for diagnosing radiative forcing and climate sensitivity. *Geophysical Research Letters*, *31*, L03205. https://doi.org/10.1029/2003GL018747

Gregory, J., & Webb, M. (2008). Tropospheric adjustment induces a cloud component in CO_2 forcing. *Journal of Climate*, *21*, 58–71. https://doi.org/10.1029/2005GL023851

Hansen, J., Sato, M., Ruedy, R., Nazarenko, L., Lacis, A., Schmidt, G. A., et al. (2005). Efficacy of climate forcings. *Journal of Geophysical Research*, *110*, D18104. https://doi.org/10.1029/2005JD005776

Heinze, R., Dipankar, A., Henken, C. C., Moseley, C., Sourdeval, O., Trömel, S., et al. (2017). Large-eddy simulations over Germany using ICON: A comprehensive evaluation. *Quarterly Journal of the Royal Meteorological Society*, *143*, 69–100. https://doi.org/10.1002/qj.2947

Ji, D., Wang, L., Feng, J., Wu, Q., Cheng, H., Zhang, Q., et al. (2014). Description and basic evaluation of Beijing Normal University Earth System Model (BNU-ESM) version 1. *Geoscientific Model Development*, 7, 2039–2064. https://doi.org/10.5194/gmd-7-2039-2014

Kamae, Y., & Watanabe, M. (2012). On the robustness of tropospheric adjustment in CMIP5 models. *Geophysical Research Letters*, 39, L23808. https://doi.org/10.1029/2012GL054275

Kamae, Y., & Watanabe, M. (2013). Tropospheric adjustment to increasing CO_2: Its timescale and the role of land-sea contrast. *Climate Dynamics*, 41, 3007–3024. https://doi.org/10.1007/s00382-012-1555-1

Kamae, Y., Watanabe, M., Ogura, T, Yoshimori, M., & Shiogama, H. (2015). Rapid adjustments of cloud and hydrological cycle to increasing CO_2: A review. *Current Climate Change Reports*, 1, 103–113. https://doi.org/10.1007/s40641-015-0007-5

Leuenberger, D., Koller, M., Fuhrer, O., & Schär, C. (2010). A generalization of the SLEVE vertical coordinate. *Monthly Weather Review*, 138, 3683–3689. https://doi.org/10.1175/2010MWR3307.1

Ma, H. Y., Chuang, C., Klein, S. A., Lo, M. H., Zhang, Y., Xie, S., et al. (2015). An improved hindcast approach for evaluation and diagnosis of physical processes in global climate models. *Journal of Advances in Modeling Earth Systems*, 7, 1810–1827. https://doi.org/10.1002/2015MS000490

Martin, G. M., Bellouin, N., Collins, W. J., Culverwell, I. D., Halloran, P. R., Hardiman, S. C., et al. (2011). The HadGEM2 family of Met office unified model climate configurations. *Geoscientific Model Development*, 4, 723–757. https://doi.org/10.5194/gmd-4-723-2011

Matsueda, M. (2011). Predictability of Euro-Russian blocking in summer of 2010. *Geophysical Research Letters*, 38, L06801. https://doi.org/10.1029/2010GL046557

Osborn, T., Conway, D., Hulme, M., Gregory, J. M., & Jones, P. D. (1999). Air flow influences on local climate: Observed and simulated mean relationships for the United Kingdom. *Climate Research*, 13, 173–191.

Rotstayn, L. D., Jeffrey, S. J., Collier, M. A., Dravitzki, S. M., Hirst, A. C., Syktus, J. I., & Wong, K. K. (2012). Aerosol- and greenhouse gas-induced changes in summer rainfall and circulation in the Australasian region: A study using single-forcing climate simulations. *Atmospheric Chemistry and Physics*, 12, 6377–6404. https://doi.org/10.5194/acp-12-6377-2012

Seidel, D. J., Zhang, Y., Beljaars, A., Golaz, J. C., Jacobson, A. R., & Medeiros, B. (2012). Climatology of the planetary boundary layer over the continental United States and Europe. *Journal of Geophysical Research*, 117, D17106. https://doi.org/10.1029/2012JD018143

Shell, K. M., Kiehl, J. T., & Shields, C. A. (2008). Using the radiative kernel technique to calculate climate feedbacks in NCAR's community atmospheric model. *Journal of Climate*, 21, 2269–2282. https://doi.org/10.1175/2007JCLI2044.1

Sherwood, S., Bony, S., Boucher, O., Bretherton, C., Forster, P., Gregory, J., & Stevens, B. (2015). Adjustments in the forcing-feedback framework for understanding climate change. *Bulletin of the American Meteorological Society*, 96, 217–228. https://doi.org/10.1175/BAMS-D-13-00167.1

Sherwood, S., Bony, S., & Dufresne, J. L. (2014). Spread in model climate sensitivity traced to atmospheric convective mixing. *Nature*, 505, 37–42. https://doi.org/10.1038/nature12829

Taylor, K. E., Stouffer, R. J., & Meehl, G. A. (2012). An overview of CMIP5 and the experiment design. *Bulletin of the American Meteorological Society*, 93(4), 485–498. https://doi.org/10.1175/BAMS-D-11-00094.1

Vial, J., Bony, S., & Dufresne, J.-L. (2013). On the interpretation of inter-model spread in CMIP5 climate sensitivity estimates. *Climate Dynamics*, 41, 3339–3362. https://doi.org/10.1007/s00382-013-1725-9

Vial, J., Bony, S., Dufresne, J.-L., & Roehrig, R. (2016). Coupling between lower-tropospheric convective mixing and low-level clouds: Physical mechanisms and dependence on convection scheme. *Journal of Advances in Modeling Earth Systems*, 8, 1892–1911. https://doi.org/10.1002/2016MS000740

Volodin, E. M., Dianskii, N. A., & Gusev, A. V. (2010). Simulating present-day climate with the INMCM4.0 coupled model of the atmospheric and oceanic general circulations. *Izvestiya, Atmospheric and Oceanic Physics*, 46, 414–431. https://doi.org/10.1134/S000143381004002X

Watanabe, M., Suzuki, T., O'ishi, R., Komuro, Y., Watanabe, S., Emori, S., et al. (2010). Improved climate simulation by MIROC5. Mean states, variability, and climate sensitivity. *Journal of Climate*, 23, 6312–6335. https://doi.org/10.1175/2010JCLI3679.1

Wu, T., Yu, R., Zhang, F., Wang, Z., Dong, M., Wang, L., et al. (2010). The Beijing Climate Center atmospheric general circulation model: Description and its performance for the present-day climate. *Climate Dynamics*, 34, 123–147. https://doi.org/10.1007/s00382-008-0487-2

Wyant, M. C., Bretherton, C. S., Blossey, P. N., & Khairoutdinov, M. (2012). Fast cloud adjustment to increasing CO_2 in a super parameterized climate model. *Journal of Advances in Modeling Earth Systems*, 4, M05001. https://doi.org/10.1029/2011MS000092

Yukimoto, S., Adachi, Y., Hosaka, M., Sakami, T., Yoshimura, H., Hirabara, M., et al. (2012). A new global climate model of the Meteorological Research Institute: MRI-CGCM3-Model description and basic performance. *Journal of the Meteorological Society of Japan*, 90A, 23–64. https://doi.org/10.2151/jmsj.2012-A02

Zelinka, M. D., Klein, S. A., Taylor, K. E., Andrews, T., Webb, M. J., Gregory, J. M., & Forster, P. M. (2013). Contribution different cloud types to feedbacks and rapid adjustments in CMIP5. *Journal of Climate*, 26, 5007–5027. https://doi.org/10.1175/JCLI-D-12-00555.1

Zhang, M., & Huang, Y. (2014). Radiative forcing of quadrupling CO_2. *Journal of Climate*, 27, 2496–2508. https://doi.org/10.1175/JCLI-D-13-00535.1